

Two-magnon Raman scattering in insulating cuprates: Modifications of the effective Raman operator

P. J. Freitas and R. R. P. Singh

Department of Physics, One Shields Avenue, University of California, Davis, California 95616-8677

(Received 15 March 2000)

Calculations of Raman scattering intensities in spin-1/2 square-lattice Heisenberg model, using the Fleury-Loudon-Elliott theory, have so far been unable to describe the broad line shape and asymmetry of the two magnon peak found experimentally in the cuprate materials. Even more notably, the polarization selection rules are violated with respect to the Fleury-Loudon-Elliott theory. There is comparable scattering in B_{1g} and A_{1g} geometries, whereas the theory would predict scattering in only B_{1g} geometry. We review various suggestions for this discrepancy and suggest that at least part of the problem can be addressed by modifying the effective Raman Hamiltonian, allowing for two magnon states with arbitrary total momentum. Such an approach based on the Sawatzky-Lorenzana theory of optical absorption assumes an important role of phonons as momentum sinks. It leaves the low-energy physics of the Heisenberg model unchanged but substantially alters the Raman line-shape and selection rules, bringing the results closer to experiments.

I. INTRODUCTION

Raman scattering provides an important tool for examining the structure of antiferromagnetic materials. Even though optical processes in Mott insulators necessarily depend on the energy bands in a complex way, the Fleury-Loudon-Elliott theory^{1,2} allows one to bypass that complexity and develop a theory for the line shape of the Raman spectra entirely within the framework of pure spin models. This theory has been highly successful in many cases and is the primary reason why the Raman scattering becomes an investigative tool for these class of materials. However, in case of the cuprates such as La_2CuO_4 , the stoichiometric parent compounds of the high-temperature superconducting materials, the Fleury-Loudon-Elliott theory runs into several difficulties. This has been a subject of intense debate, and many explanations have been proposed ranging from the inadequacy of the theory to novel and exotic microscopic physics in these materials. The goal of this paper is to review the various explanations and to examine how far a simple modification to the effective ‘‘Raman Hamiltonian’’ that allows two-magnon states with arbitrary total momentum, can help bridge the gap between theory and experiments.

It is fair to say that Raman scattering provided some of the earliest accurate estimates for the antiferromagnetic exchange constant in the cuprates.⁴ This, by itself, is proof that the peak-frequency of the Raman scattering intensity matches reasonably with theoretical expectations. Furthermore, the line shape of the spectra is reasonably universal from one material to another within the insulating cuprates,^{5–8} and although there are details in the shape whose dependence on the incident photon energy can be clearly recognized, the gross features of the line shape are largely independent of such resonance effects. Thus the discrepancy between theory and experiment only come in when a more detailed calculation of the line shape is performed within the Fleury-Loudon-Elliott theory. The experimental spectra is much broader, perhaps by about a factor of 3, and has a clear

asymmetry extending towards high energies. The most notable discrepancy with the theory is that in the experiments there is comparable scattering intensity in A_{1g} and B_{1g} polarizations of incident and outgoing light, whereas theory predicts scattering predominantly in B_{1g} geometry only. The fact that the main features of the spectra are so universal suggests that it is intrinsic and significant.

The theoretical work focusing on these discrepancies can be grouped into the following categories:

(i) Inaccuracies of numerical calculations: Even given a system well described by a nearest-neighbor Heisenberg model and an effective spin Hamiltonian which describes the Raman scattering process, the calculation of Raman-scattering line shape remains a challenging task. The spin-wave theory,⁹ which works well for higher spin and higher dimensional systems, need not be accurate for a two-dimensional (2D) spin-half system. Improved calculations have involved higher-order spin-wave theory,¹⁰ series expansions,¹¹ exact-diagonalization of small systems,¹² and finite temperature quantum Monte Carlo simulations.¹³ These calculations have established the first few moments of the spectra quite well. The quantum Monte Carlo calculation is perhaps the best in terms of getting the line shape correct and suggests that the actual line shape can be fairly different from spin-wave theory. It may be both broader than spin-wave theory and have some of the high-energy asymmetry, but perhaps not as much as in the experiments.

(ii) The Heisenberg model is not good enough for the cuprates: Other work has focused on extending the nearest-neighbor Heisenberg model in order to get better agreement with the experiments. For example, one could introduce second neighbor antiferromagnetic interactions to explain scattering in A_{1g} geometries.¹¹ A more radical proposal has been the possibility of substantial or dominant ring-exchange terms,^{14,15} which can dramatically broaden the spectra. The consistency of such an approach with other measurements (most notably neutron scattering) has not been shown.

(iii) Line shape depends on resonance: Chubukov and Frenkel¹⁶ and independently Kampf *et al.* have argued that

the line shape does depend on the frequency of incident photon energy^{17,18} and these features can also make the spectra appear broader and give enhanced scattering at higher frequencies.

(iv) Other degrees of freedom, most notably phonons are important: It has been argued by several authors that coupling between spin and phonons can lead to substantial broadening of the spectra. Calculations in this respect have included modeling phonons by substantial modulation of local coupling constants¹⁹ as well as by spin-wave theory.²⁰ Again, the consistency of strong spin-phonon couplings to neutron scattering and other measurements have not been shown. In particular, the fact that neutron-scattering measurements, especially the temperature-dependent correlation length $\xi(T)$ and the spin dynamics, agree remarkably well with the Heisenberg model^{21,22} does not leave room for such couplings.

(v) Magnons are not good elementary excitations at short wavelengths: One of the most exciting suggestions from a physics point of view has been to invoke spinons and not magnons as elementary excitations of the system, at least at short wavelengths.^{23–26} Such an approach naturally leads to a much broader spectra, and can be considered to be successful at a phenomenological level. The primary difficulty with this approach is that the existence of spinonlike excitations in two dimensions remains highly controversial.

(vi) The need to go beyond the spin-subspace to describe the scattering process: The work of Shastry and Shraiman²⁷ has presented a comprehensive theoretical framework for understanding the Fleury-Loudon-Elliott scheme for effective Raman Hamiltonians starting from an electronic Hamiltonian. However, the cuprate materials are far from the large- U limit where such a scheme can be rigorously shown to work, and thus multiple bands and detailed band structure may play a role here. However, as noted before, the fact that the spectral features are reasonably universal over different family of materials suggests a more generic explanation may be appropriate.

In this paper, we primarily concern ourselves with the numerical calculation of the Raman-scattering line shape with a modified effective Hamiltonian. Such an approach does not alter the ground-state properties and elementary excitations of the system, but only the way in which the Raman scattering process is described within the spin subspace. The basic idea is based on the work of Sawatzky and Lorenzana²⁸ for optical absorption in the cuprates. They argued that the optical absorption was assisted by phonons, whose role can be incorporated into the theory by simply assuming that they acted as momentum sinks. Thus optical absorption could proceed through excitation of two magnons with arbitrary total momentum. Here we explore the analogous situation for Raman scattering aided by phonons. This immediately leads to scattering in both B_{1g} and A_{1g} geometries. Furthermore, the spectral features come closer to experiments. Given our finite-size numerical calculations, it is difficult to say whether these are now in complete agreement with experiments.

II. PHONON-ASSISTED SCATTERING: THE SINGLE-SITE OPERATOR (SSO)

Let us first examine the rationale behind the very successful Fleury-Loudon¹ theory as formulated by Elliott.² Al-

though Raman scattering proceeds through virtual charge excitations, the scattering process can be described by an effective spin Hamiltonian, simply by incorporating the important symmetries of the problem. This is possible because the initial and final states both lie well below the charge gap and thus the resulting excitation must be a pure spin excitation. Since light has very long wavelength and the scattering involves the electric field and not the magnetic field, the effective Raman Hamiltonian must have zero total momentum and be a spin singlet. It must be linear in the polarizations of incoming and outgoing electric-field vectors and must be a scalar. If we further assume the dominance of nearest-neighbor superexchange, the effective Raman Hamiltonian is essentially fully determined apart from an overall multiplicative constant. It takes the Fleury-Loudon-Elliott form

$$\mathcal{H}_R = \sum_{\langle ij \rangle} (\vec{\epsilon}_{in} \cdot \hat{r}_{ij})(\vec{\epsilon}_{out} \cdot \hat{r}_{ij}) \vec{S}_i \cdot \vec{S}_j. \quad (1)$$

where the sum runs over the nearest-neighbor pairs, ϵ_{in} and ϵ_{out} are the incoming and outgoing electric-field polarization vectors, and \hat{r}_{ij} is a unit vector connecting the sites i and j .

Thus in the B_{1g} configuration, where the incoming and outgoing light are polarized in the plane of the copper oxides at right angles to each other and at an angle 45° from the x and y axes of the CuO_2 lattice, the effective scattering operator becomes

$$O_{B_{1g}} = \sum_{\langle ij \rangle, x} \vec{S}_i \cdot \vec{S}_j - \sum_{\langle ij \rangle, y} \vec{S}_i \cdot \vec{S}_j, \quad (2)$$

where the first sum is over the nearest neighbor bonds parallel to the x axis, and the second sum is over the nearest neighbor bonds parallel to the y axis.

In contrast, the effective Hamiltonian vanishes in the B_{2g} configuration, where the incoming and outgoing light are polarized in the plane of the copper oxides at right angles to each other, with one being along the x and the other along the y axis. In the A_{1g} configuration, the Fleury-Loudon-Elliott operator becomes

$$O_{A_{1g}} = \sum_{\langle ij \rangle, x} \vec{S}_i \cdot \vec{S}_j + \sum_{\langle ij \rangle, y} \vec{S}_i \cdot \vec{S}_j, \quad (3)$$

which is just the Heisenberg Hamiltonian and, thus, results in no scattering. Thus the theory predicts scattering in B_{1g} geometry only. The spectra obtained by treating this effective Hamiltonian in the two magnon approximation for $S \geq 1$, provide a remarkably accurate description of the experiments in K_2NiF_4 and other materials.³ Numerical calculations for $S = 1/2$, and their lack of agreement with the cuprate materials will be discussed in the following sections.

Here we will examine the possibility that the phonons or impurities play an important role in the Raman-scattering process, even though they do not much effect the system in the absence of incident light. One way to mimic the role of phonons follows from the work of Lorenzana and Sawatzky²⁸ on optical absorption in antiferromagnets. The key effect of phonons, in their theory, is to act as a momentum sink, allowing absorption via two-magnon states of ar-

bitrary total momentum. This theory has proved to be very successful in describing optical absorption in the quasi-1D material Sr_2CuO_3 .²⁹

We can incorporate this idea of phonons acting as momentum sinks in Raman scattering by modifying the Raman scattering operator. The most natural choice is to consider the following single-site operator (SSO) for the B_{1g} configuration:

$$O_{B_{1g}} = \sum_{\langle j \rangle, x} \vec{S}_0 \cdot \vec{S}_j - \sum_{\langle j \rangle, y} \vec{S}_0 \cdot \vec{S}_j, \quad (4)$$

and, for the A_{1g} configuration:

$$O_{A_{1g}} = \sum_{\langle j \rangle, x} \vec{S}_0 \cdot \vec{S}_j + \sum_{\langle j \rangle, y} \vec{S}_0 \cdot \vec{S}_j. \quad (5)$$

Notice that the latter no longer commutes with the antiferromagnetic Heisenberg Hamiltonian, and can thus produce scattering in the A_{1g} channel. In general, one would expect that by including two magnons at arbitrary momentum the two magnons will scatter less with each other in the final state and thus lead to a broadening of the spectra. Whether this effect combined with quantum fluctuations can lead to a spectra consistent with the experiments becomes a numerical issue.

III. COMPUTATIONAL METHODS

Results shown in this paper will be based on exact diagonalization computations of Raman spectra. The antiferromagnetic Heisenberg model is used for systems of 16 and 26 sites. To obtain a ground-state vector $|\psi_0\rangle$ having energy E_0 , a conjugate gradient method was used.³⁰ Once that was accomplished, it was possible to compute zero-temperature Raman spectra using a variety of methods, which we will now discuss. Let us assume that our scattering operator is O ; the equation for the scattering intensity I at the shifted frequency ω has the form

$$I(\omega) = -\frac{1}{\pi} \text{Im} \left[\left\langle \psi_0 \left| O^\dagger \frac{1}{\omega + E_0 + i\epsilon - H} O \right| \psi_0 \right\rangle \right], \quad (6)$$

where H is the Hamiltonian of the system and ϵ is a small real number introduced to allow computation. This equation can also be expressed in a Fermi's golden rule form,

$$I(\omega) = \sum_n |\langle \psi_n | O | \psi_0 \rangle|^2 \delta[\omega - (E_n - E_0)], \quad (7)$$

where $|\psi_n\rangle$ and E_n are eigenvectors and eigenvalues of the system.

There are many possible ways to perform this calculation using these two equation forms. One standard method is to use a continued fraction calculation on the first form. Dagotto¹² describes how this calculation can be performed. More recent techniques relying on the second form of the scattering equation are simpler to implement, however. The first one we shall examine, which is sometimes called the spectral decoding technique, was introduced by Loh and

Campbell.³¹ Let us define a set of vectors $|\phi_n\rangle$ using the well-known Lanczös iteration technique:³²

$$|\phi_0\rangle = \frac{O|\psi_0\rangle}{\sqrt{\langle \psi_0 | O^\dagger O | \psi_0 \rangle}}, \quad (8)$$

$$|\phi_1\rangle = H|\phi_0\rangle - \frac{\langle \phi_0 | H | \phi_0 \rangle}{\langle \phi_0 | \phi_0 \rangle} |\phi_0\rangle, \quad (9)$$

and

$$|\phi_{n+1}\rangle = H|\phi_n\rangle - \frac{\langle \phi_n | H | \phi_n \rangle}{\langle \phi_n | \phi_n \rangle} |\phi_n\rangle - \frac{\langle \phi_n | \phi_n \rangle}{\langle \phi_{n-1} | \phi_{n-1} \rangle} |\phi_{n-1}\rangle. \quad (10)$$

With this set of vectors defined, we now have a simple tridiagonal form for the Hamiltonian matrix that can be easily diagonalized. We can now say that the eigenvectors $|\psi_n\rangle$ are related to the $|\phi_n\rangle$ by the relationship

$$|\psi_n\rangle = \sum_m c_m^n |\phi_m\rangle. \quad (11)$$

It can now be shown that

$$|\langle \psi_n | O | \psi_0 \rangle|^2 = |c_0^n|^2 \langle \psi_0 | O^\dagger O | \psi_0 \rangle. \quad (12)$$

The final spectrum can be displayed by replacing the Dirac delta functions in Eq. (7) with finite Lorentzians of an arbitrary width.

Spectral decoding is a very useful technique, but it has some disadvantages. It relies on the Lanczös method for eigenvector computation above the ground state, and it is known that the Lanczös method can produce eigensolutions which are either incorrect or are duplicates of other solutions found previously. Techniques exist for checking the validity of solutions provided by the Lanczös method,³² which we shall call sorting, but they can be cumbersome. It would be preferable to use another technique where sorting is not necessary.

For the spectra computed in this paper, the kernel polynomial method³³ (KPM) was used. In KPM, a convergent approximation to the true spectrum is computed using Chebyshev polynomials. The delta function in Eq. (7) is replaced with a Chebyshev expansion of the delta function, and Gibbs damping factors are included to eliminate the Gibbs phenomenon. Calculations are performed using the operator X instead of H , where X is simply rescaled so that all energies lie between -1 and 1 . Similarly, we use x instead of ω , where x is ω rescaled to lie between 0 and 2 . The final calculation involved is

$$I(x) = \frac{1}{\pi \sqrt{1 - (x-1)^2}} \left[g_0 \mu_0 + 2 \sum_m g_m T_m(x-1) \mu_m \right], \quad (13)$$

where the T_m are Chebyshev polynomials, the g_m are Gibbs damping factors, and the moments μ_m are defined by

$$\mu_m = \langle \psi_0 | O^\dagger T_m(X) O | \psi_0 \rangle. \quad (14)$$

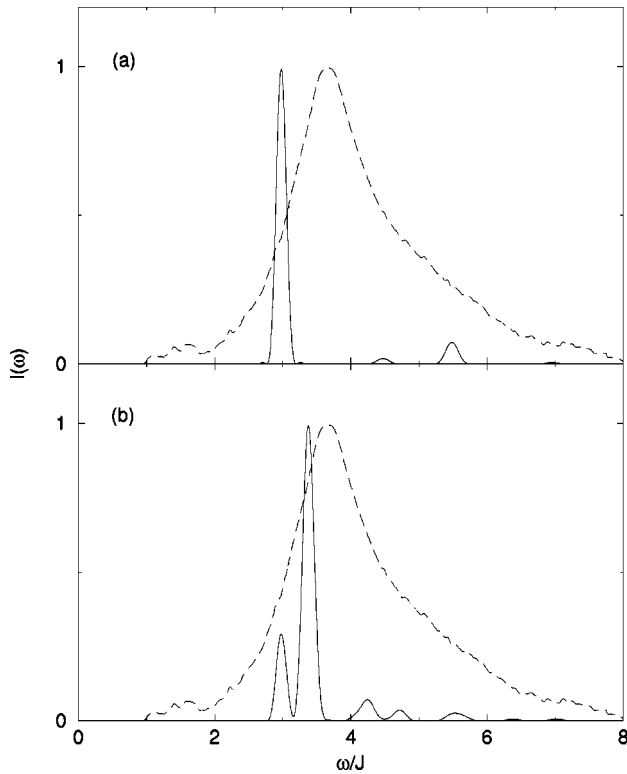


FIG. 1. (a) 16 site Fleury-Loudon-Elliott type B_{1g} scattering spectrum (solid) compared with experiment (dashed). (b) Single-site operator scattering for the same system (solid) compared with experiment (dashed).

The $T_m(X)$ here are Chebyshev polynomials of the operator X . In practice, the moments are most easily calculated using Chebyshev recurrence relations. Using these relations, computing M moments requires only $M/2+1$ calculations.

KPM results are equivalent to those of other methods mentioned above. KPM is used here because it is simpler to implement computationally than other methods for a given level of accuracy.

IV. RESULTS

Now let us examine some of our results. Calculations for the 16 site model were performed on a 200-MHz personal computer. The Néel state was used as a starting point for ground state calculations. Spin-flip symmetry was used to reduce the final size of the Hilbert space to 6435. Memory requirements were minimal, and calculations were accomplished in minutes. The 26 site system spectra were computed on various machines with Alpha processors. Again, a spin-flip symmetry was the only symmetry used, the Néel state was used as an initial approximation to the ground state, and the Hilbert space had a dimensionality of 5 200 300. Several hundred megabytes of RAM were required, and the calculations were completed in several hours time.

Figure 1 shows some computed spectra in the B_{1g} configuration for a 16 site Heisenberg model of the square lattice with periodic boundary conditions. If we examine the Fleury-Loudon-Elliott spectrum [the solid curve in part (a)] and the SSO spectrum [the solid curve in part (b)] we see that there is much more activity in the SSO spectrum, and

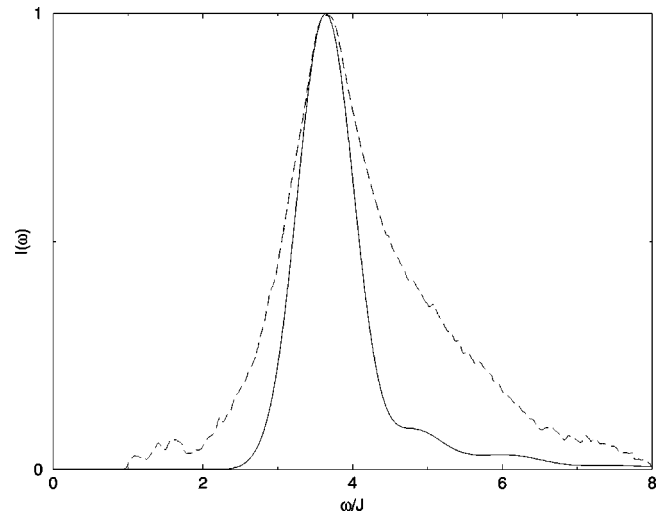


FIG. 2. The SSO spectrum of Fig. 1(b) broadened and shifted slightly (solid) to demonstrate the goodness of fit with experiment (dashed).

that its greatest activity occurs more toward the peak determined by experiment¹¹ for La_2CuO_4 (dashed curves). In Fig. 2, we see the SSO spectrum broadened and shifted slightly so that its main peak is in the same location as the experimental curve. Here we see that the spectrum is beginning to resemble the experimentally determined one fairly closely, with its characteristic asymmetry. In the computed A_{1g} spectrum from the single-site operator, we find even more encouraging results. For a 16 site model, the SSO spectrum shown in Fig. 3 is peaked at almost exactly the same location (about 4.2 J) as the experimentally determined spectrum. The scaling used here is the same scaling used to match the peak heights for the B_{1g} spectrum. It is interesting to note that this scaling, chosen independently of the A_{1g} results, puts the peak at exactly the correct height.

We find similarly encouraging results with a 26 site model. In Fig. 4, we again see the B_{1g} spectra for the SSO [solid curve of part (a)] and the Fleury-Loudon-Elliott opera-

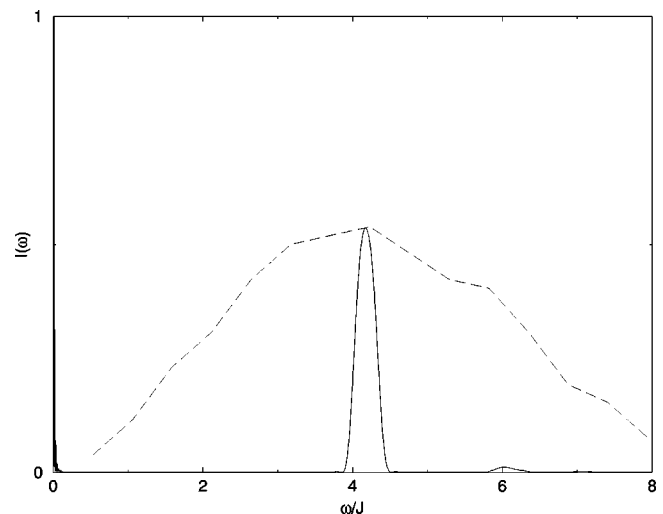


FIG. 3. The 16 site SSO A_{1g} spectrum compared with a sketch of the experimental data. Note that no shifting is necessary in this example.

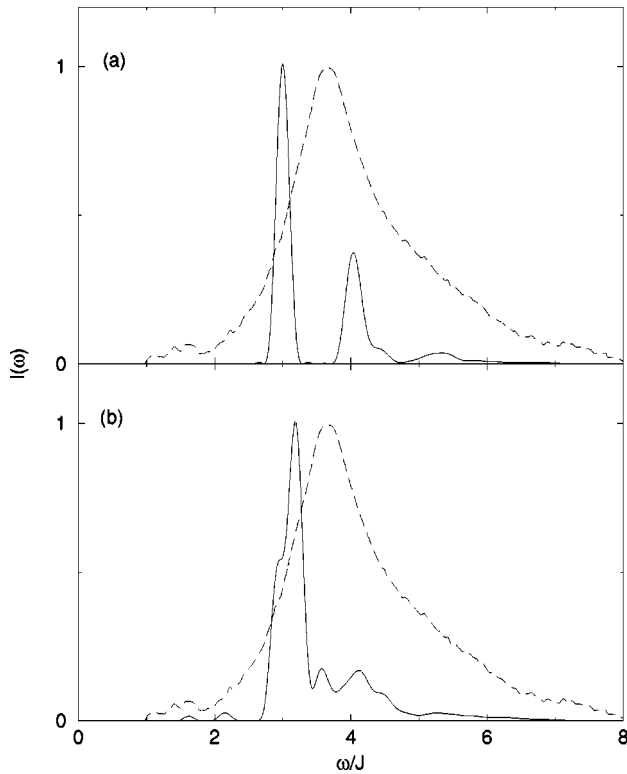


FIG. 4. (a) 26 site Fleury-Loudon-Elliott type B_{1g} scattering spectrum (solid) compared with experiment (dashed). (b) Single-site operator scattering for the same system (solid) compared with experiment (dashed).

tor [solid curve, part (b)] compared with experiment for La_2CuO_4 (dashed curves). Again we see that the SSO spectrum has more activity in better proportions than the Fleury-Loudon-Elliott curve does. The two magnon peak (the maximum) is shifted slightly closer to what experiment shows, and there is more broadly distributed four magnon activity in the SSO curve. In short, the asymmetry and line broadening seen in experiment is better suggested by the SSO spectrum than by the pure Fleury-Loudon-Elliott spectrum. If we again broaden the SSO spectrum and shift it slightly, in the same manner as for the 16 site model, we see in Fig. 5 that we have a better approximation of the experimentally-determined spectrum. In the A_{1g} spectrum shown in Fig. 6, we see the same encouraging signs of extra activity from a larger model, as compared with Fig. 3.

Lastly, it should be pointed out that the goodness of the fit does appear to improve with increased system size. It would be helpful to see these calculations performed for larger systems. The SSO lacks translational symmetry, unfortunately, which prohibits many reductions in Hilbert space size that would otherwise be possible. For the moment, exact diagonalization of larger systems is beyond the capabilities of the authors' computing facilities. Only the quantum Monte Carlo method¹³ can deal with substantially larger sizes and should prove specially informative.

V. CONCLUSION

In this paper, we have presented numerical data from exact-diagonalization studies that suggest that improved understanding of magnetic Raman scattering in the insulating

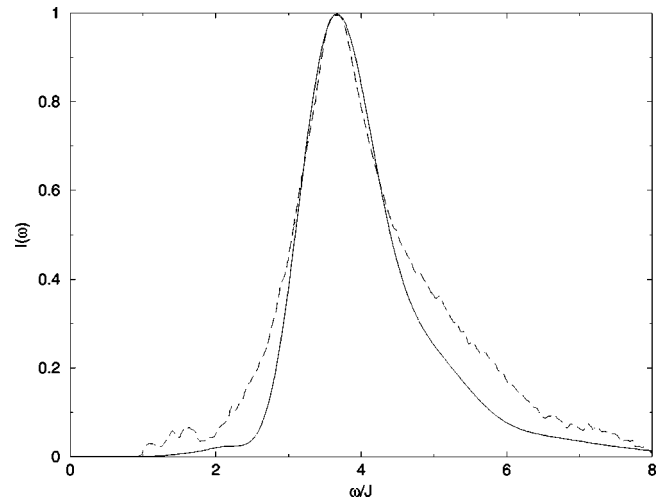


FIG. 5. The SSO spectrum of Fig. 4(b) broadened and shifted slightly (solid) to demonstrate the goodness of fit with experiment (dashed).

cuprates can result from a modification of the Fleury-Loudon-Elliott Raman operator. This assumes that phonons participate in the Raman-scattering process, acting as momentum sinks and allowing for Raman scattering from two magnon states with arbitrary total momentum. This provides a natural explanation for comparable Raman scattering in A_{1g} and B_{1g} configurations, and leads to a broadening of the spectra. This is achieved without invoking substantial modulations of local exchange constants, which can strongly effect long-wavelength properties. Due to limitations of sizes, the results presented are not fully conclusive about how close this brings the theoretical results to the experiments. Quantum Monte Carlo simulations may prove helpful in this regard.

Given the large number of experiments on insulating cuprates, which can be modeled in terms of the square-lattice Heisenberg model, with a single nearest-neighbor exchange constant J , it seems natural that this be regarded as a good model for this system unless clear evidence to the contrary emerges. Raman scattering by itself cannot be invoked to

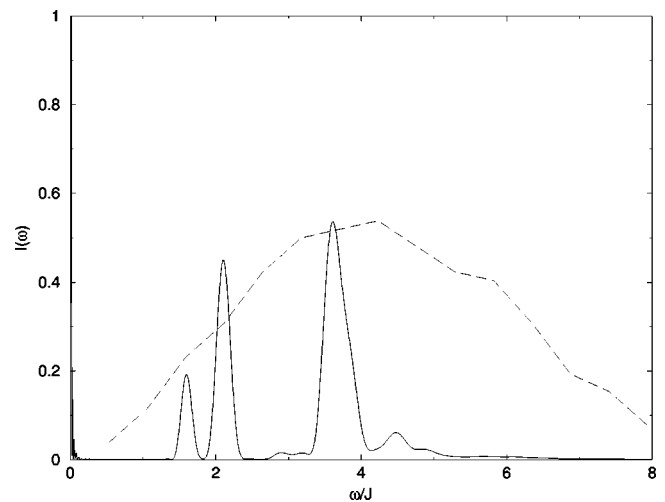


FIG. 6. The 26 site SSO A_{1g} spectrum (solid) compared with a sketch of the experimental data (dashed).

justify more fancy terms such as ring-exchange terms for these systems. Raman scattering is also not the ideal ground for establishing the existence of spinons and other exotic excitations, although in the cuprates it definitely leaves room for such exotic physics. More direct probes of quasiparticles, photoemission, and neutron scattering can be more persuasive in this regard.

ACKNOWLEDGMENTS

This work was supported in part by the Campus Laboratory Collaboration of the University of California and by the National Science Foundation under Grant No. DMR-9986948. Computations were carried out at Lawrence Livermore National Laboratory.

-
- ¹P.A. Fleury and R. Loudon, Phys. Rev. **166**, 514 (1968).
²R.J. Elliott and R. Loudon, Phys. Lett. **3**, 189 (1963).
³J.B. Parkinson, J. Phys. C **2**, 2012 (1969).
⁴K.B. Lyons, P.E. Sulewski, P.A. Fleury, H.L. Carter, A.S. Cooper, G.P. Espinosa, Z. Fisk, and S.-W. Cheong, Phys. Rev. B **39**, 9693 (1989).
⁵K.B. Lyons, P.A. Fleury, J.P. Remeika, A.S. Cooper, and T.J. Negran, Phys. Rev. B **37**, 2353 (1988).
⁶K.B. Lyons, P.A. Fleury, L.F. Schneemeyer, and J.V. Waszczak, Phys. Rev. Lett. **60**, 732 (1988).
⁷S. Sugai, S. Shamoto, and M. Sato, Phys. Rev. B **38**, 6436 (1988).
⁸S. Sugai and Y. Hidaka, Phys. Rev. B **44**, 809 (1991).
⁹D.K. Morr and A.V. Chubukov, Phys. Rev. B **56**, 9134 (1997).
¹⁰C.M. Canali and S.M. Girvin, Phys. Rev. B **45**, 7127 (1992).
¹¹R.R.P. Singh, P.A. Fleury, K.B. Lyons, and P.E. Sulewski, Phys. Rev. Lett. **62**, 2736 (1989).
¹²E. Dagotto, Rev. Mod. Phys. **66**, 763 (1994).
¹³A.W. Sandvik, S. Capponi, D. Poilblanc, and E. Dagotto, Phys. Rev. B **57**, 8478 (1998).
¹⁴M. Roger and J.M. Delrieu, Phys. Rev. B **39**, 2299 (1989).
¹⁵J. Lorenzana, J. Eroles, and S. Sorella, Phys. Rev. Lett. **83**, 5122 (1999).
¹⁶A.V. Chubukov and D.M. Frenkel, Phys. Rev. B **52**, 9760 (1995).
¹⁷F. Schönfeld, A.P. Kampf, and E. Müller-Hartmann, Z. Phys. B: Condens. Matter **102**, 25 (1997).
¹⁸G. Blumberg, P. Abbamonte, M.V. Klein, W.C. Lee, D.M. Ginsberg, L.L. Miller, and A. Zibold, Phys. Rev. B **53**, R11 930 (1996).
¹⁹F. Nori, R. Merlin, S. Haas, A.W. Sandvik, and E. Dagotto, Phys. Rev. Lett. **75**, 553 (1995).
²⁰J.D. Lee and B.I. Min, J. Phys. Soc. Jpn. **66**, 442 (1997).
²¹Y. Endoh, K. Yamada, R.J. Birgeneau, D.R. Gabbe, H.P. Jenssen, M.A. Kastner, C.J. Peters, P.J. Picone, T.R. Thurston, M. Tranquada, G. Shirane, Y. Hidaka, M. Oda, Y. Enomoto, M. Suzuki, and T. Murakami, Phys. Rev. B **37**, 7443 (1988).
²²S. Chakravarty, B.I. Halperin, and D.R. Nelson, Phys. Rev. B **39**, 2344 (1989).
²³T.C. Hsu, Phys. Rev. B **41**, 11 379 (1990).
²⁴Y.R. Wang, M.J. Rice, and H.Y. Choi, Phys. Rev. B **44**, 9743 (1991).
²⁵Y.R. Wang, Phys. Rev. B **43**, 3786 (1991).
²⁶Y.R. Wang, Phys. Rev. B **43**, 13 774 (1991).
²⁷B.S. Shastry and B.I. Shraiman, Phys. Rev. Lett. **65**, 1068 (1990).
²⁸J. Lorenzana and G.A. Sawatzky, Phys. Rev. B **52**, 9576 (1995).
²⁹J. Lorenzana and R. Eder, Phys. Rev. B **55**, R3358 (1997).
³⁰M.P. Nightingale, V.S. Viswanath, and G. Müller, Phys. Rev. B **48**, 7696 (1993).
³¹E.Y. Loh and D.K. Campbell, Synth. Met. **27**, A499 (1988).
³²J. K. Cullum and R. A. Willoughby, *Lanczos Algorithms for Large Symmetric Eigenvalue Computations* (Birkhäuser, Boston, 1985).
³³R.N. Silver, H. Röder, A.F. Voter, and J.D. Kress, J. Comput. Phys. **124**, 115 (1996).